Cell Stem Cell, Volume *26*

Supplemental Information

Distinct Mesenchymal Cell Populations Generate the Essential Intestinal BMP Signaling Gradient

Neil McCarthy, Elisa Manieri, Elaine E. Storm, Assieh Saadatpour, Adrienne M. Luoma, Varun N. Kapoor, Shariq Madha, Liam T. Gaynor, Christian Cox, Shilpa Keerthivasan, Kai Wucherpfennig, Guo-Cheng Yuan, Frederic J. de Sauvage, Shannon J. Turley, and Ramesh A. Shivdasani

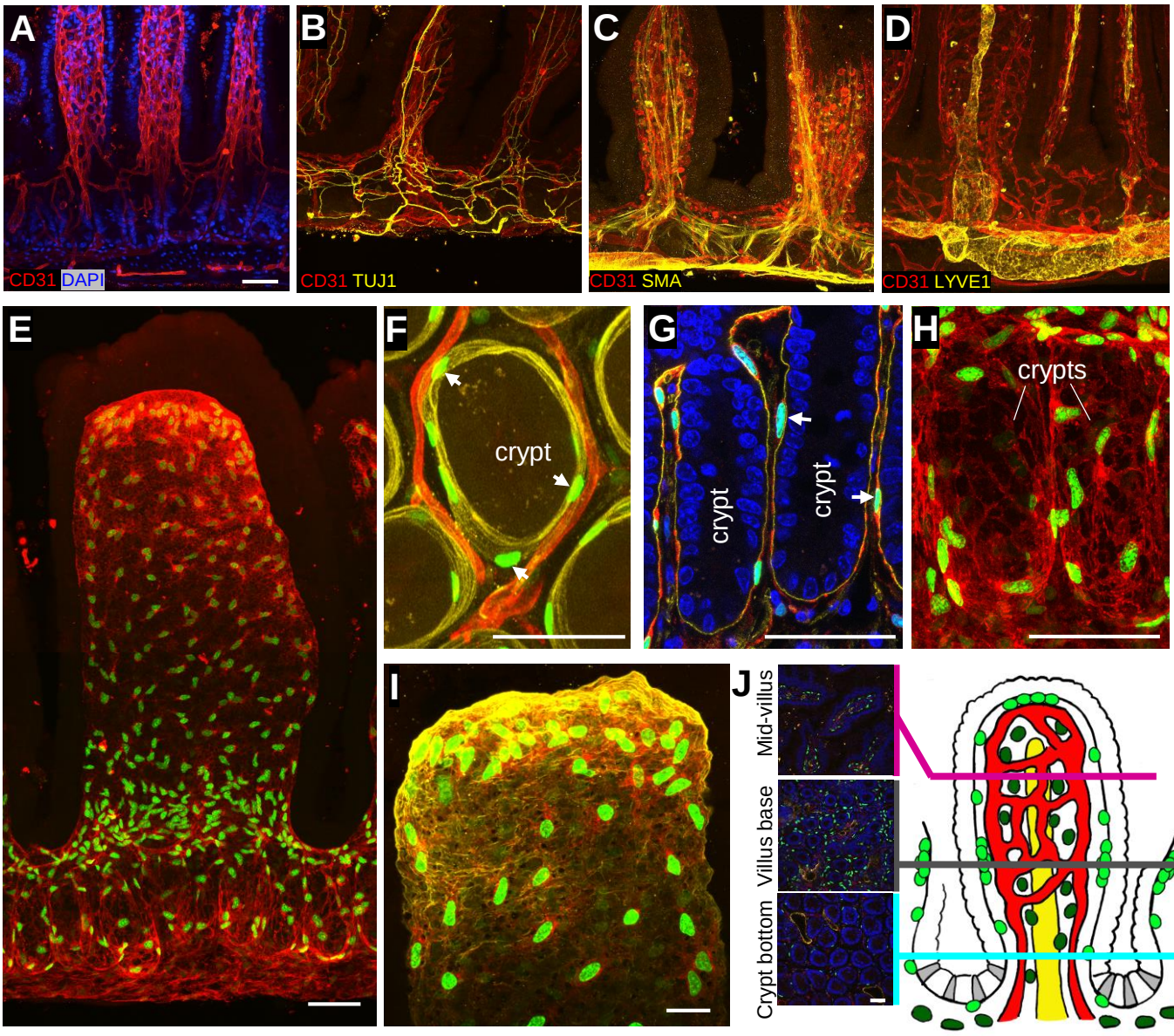
A
CD31 DAPI
B
CD31 TUJ1
C
CD31 SMA
D
CD31 LYVE1
E
F
crypt
G
crypt
crypt
H
crypts
I
J
Mid-villus
Villus base
Crypt bottom

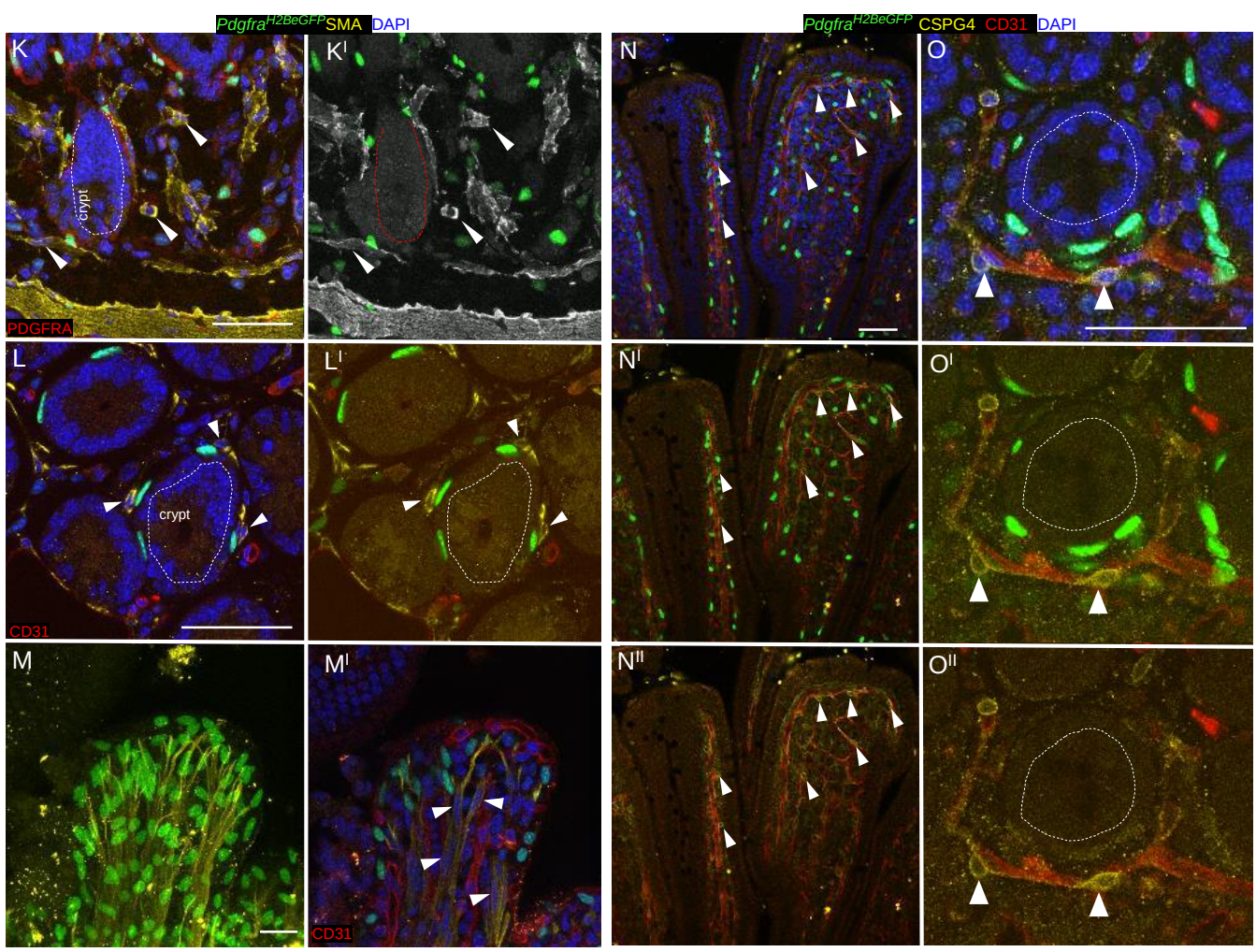
PdgfraH2BeGFP SMA DAPI
K
KI
crypt
PDGFRA
L
LI
crypt
CD31
M
MI
CD31
PdgfraH2BeGFP CSPG4 CD31 DAPI
N
O
NI
OI
NII
OII

Figure S1. Stereotypical architecture of small intestine mesenchyme (Related to Figure 1)**.**

(A-D) 3D-rendered images of small intestinal mesenchyme components, including the $CD31^+$ vascular plexus (A), which forms a sub-epithelial sheath enclosing $TUJ1^+$ neural projections (B), smooth muscle actin $(SMA)^+$ myofibroblasts (C), and $LYVE1^+$ lymphatic (lacteal, D) vessels.

(E) 3D-rendered image showing the distribution of *Pdgfra*^{H2BEGFP} cells along entire crypt-villus axis. Image is a composite of two overlaid images. Green, GFP^+ nuclei; red, PDGFRA Ab stain.

(F-G) Transverse (F) and longitudinal (G) tissue sections through the crypt zone, showing GFP^{hi} telocytes (arrows) embedded in the $Laminin^+$ basement membrane present between the blood vessels and epithelium. red=Cd31(F), PDGFRA(G), yellow=laminin

(H-I) 3D-rendered images of crypts (H) and a representative villus tip (I), showing that GFP^{hi} telocytes express PDGFRA(red) and embrace the epithelium with an extensive web-like cytoplasm. yellow=laminin.

(J) Still images from Video 2, illustrating the relative abundance of telocytes (GFP^{hi}) at the villus base, compared to the crypt surface.

(K-L) *Pdgfra*^{H2BeGFP} mouse intestines stained for smooth-muscle actin (SMA, yellow), with the crypt zone shown in vertical (K-K') and transverse (L-L') sections. SMA^+ cytoplasm and GFP^+ nuclei are in different cells (arrowheads: SMA^+ GFP^- cells); $CD31^+$ blood vessels are stained red.

(M) 3D-rendered image of a villus tip. Arrowheads point to cells with SMA^+ cytoplasm and GFP^- nuclei. Conversely, GFP^+ nuclei are not associated with SMA^+ cytoplasm.

(N-O) *Pdgfra*^{H2BeGFP} mouse intestines stained for the pericyte marker CSPG4 and vascular marker CD31, shown in representative villi (D-D") and crypts (E-E"). Dotted lines demarcate the epithelium and arrowheads point to $CSPG4^+$ cells with GFP^- nuclei. All scale bars, 50 μm.

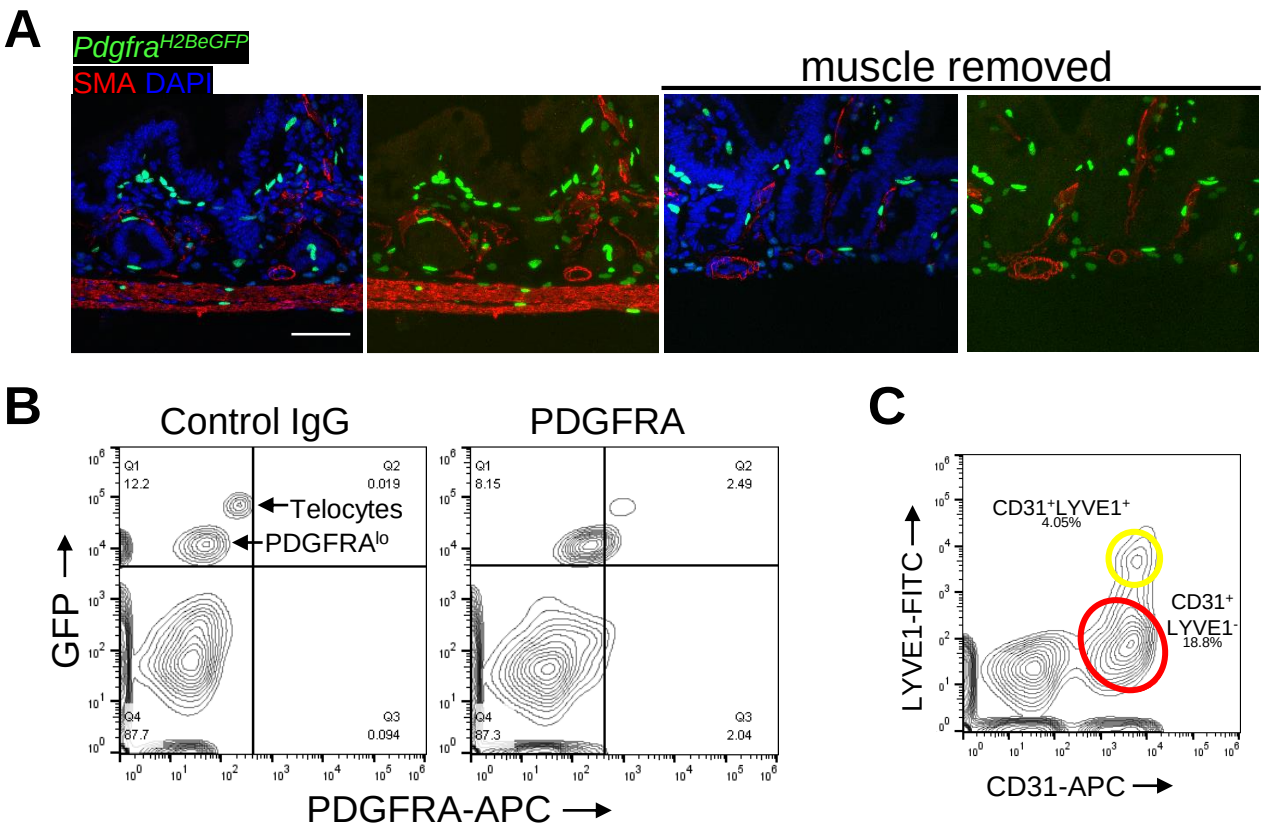
A
Pdgfra H2BeGFP
SMA DAPI
muscle removed
B
Control IgG
PDGFRA
Q1 12.2
Q2 0.019
Q4 87.7
Q3 0.094
Q1 8.15
Q2 2.49
Q4 87.3
Q3 2.04
Telocytes
PDGFRA lo
GFP
PDGFRA-APC
C
CD31+LYVE1+ 4.05%
CD31+ LYVE1- 18.8%
LYVE1-FITC
CD31-APC
D
Lgr5+ ISC
Paneth
Ent-Pro
Telocytes
PDGFRA lo
EC
LEC
1 0.98 0.96 0.96 0.95 0.95 0.76 0.77 0.75 0.77 0.79 0.79 0.79 0.79
1 0.97 0.97 0.96 0.96 0.77 0.78 0.76 0.78 0.79 0.79 0.79 0.79
1 0.97 0.95 0.95 0.77 0.78 0.77 0.79 0.8 0.8 0.79 0.79
1 0.96 0.96 0.77 0.77 0.76 0.78 0.79 0.79 0.78 0.78
1 0.99 0.79 0.79 0.78 0.81 0.81 0.81 0.81 0.82
1 0.79 0.79 0.79 0.81 0.83 0.82 0.82 0.83
1 0.99 0.94 0.93 0.86 0.86 0.84 0.86
1 0.93 0.93 0.86 0.86 0.84 0.86
1 0.97 0.9 0.91 0.87 0.9
1 0.9 0.9 0.88 0.9
1 0.97 0.94 0.94
1 0.93 0.93
1 0.98
1
E
PC2 (18%)
PC1 (71%)
F
P0: +rNOGGIN +rRSPO1 (no mesenchymal cells)
Passage 1: +rNOGGIN +rRSPO1
102 ±11 secondary organoids
P0: + PDGFRA lo cells
8 ±3 secondary organoids

Figure S2. Molecular and functional characteristics of isolated small intestinal stromal cell types (Related to Figure 2)**.**

(A) Manual stripping of outer intestinal muscle layers to remove strongly SMA^+ cells and intramuscular $PDGFRA^+$ (GFP^+) cells, leaving mesenchymal $PDGFRA^+$ cells intact for isolation by flow cytometry. Scale bar, 50 μm.

(B) Two-color FACS plot of *Pdgfra*^{H2BeGFP} mesenchymal cells with GFP (y-axis) and PDGFRA Ab stain (APC, x-axis). By this method, PDGFRA Ab recognizes telocytes and a fraction of $PDGFRA^{lo}$ cells, without sufficient discrimination from each other or from $PDGFRA^-$ cells to allow replicable FACS isolation.

(C) FACS plot showing isolation of $CD31^+LYVE1^+$ (yellow circle) lymphatic and $CD31^+LYVE1^-$ (red circle) vascular endothelial cells.

(D) Pearson correlations among duplicate RNA-seq libraries prepared from ISC, Paneth cells, enterocyte progenitors (Ent-Pro), telocytes, $PDGFRA^{lo}$ cells, and blood (EC) or lymphatic (LEC) endothelial cells. The two $PDGFRA^+$ cell types are substantially different from each other and from the other populations. ISC, intestinal stem cells; Ent-Pro, enterocyte progenitors; EC, blood endothelial cells; LEC, lymphatic endothelial cells

(E) Principal Component (PC) analysis of duplicate RNA profiles of the indicated cell types. Epithelial cells cluster separately from mesenchymal cells and, among the latter, endothelial cells and $PDGFRA^+$ cells cluster separately. Colors correspond with D.

(F) Passage (P1) of enteroid structures in complete ENR medium (rEGF, rNOGGIN, rRSPO1) (Sato et al., 2009) after initial growth (P0) in the indicated conditions and disaggregation before passage. Crypts initially grown with recombinant factors and no mesenchymal cells passaged robustly (inset magnifies the boxed area), whereas enteroids from $PDGFRA^{lo}$ co-cultures passaged poorly (*N*=3 experiments, significance tested by two-tailed t-test, *P*<0.0001). Scale bars, 1 mm.

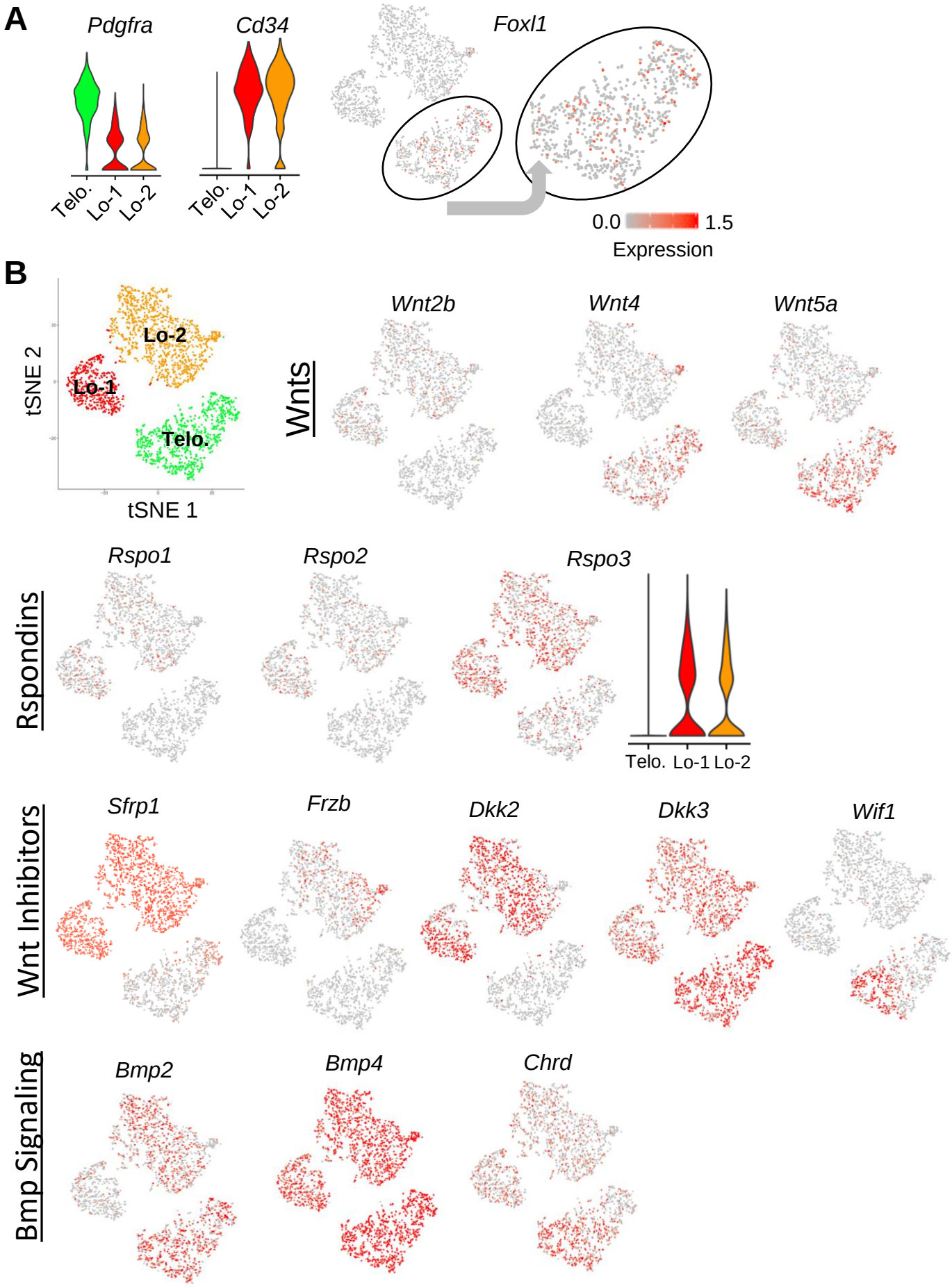
A
Pdgfra
Cd34
Foxl1
Telo.
Lo-1
Lo-2
0.0
1.5
Expression
B
tSNE 2
tSNE 1
Lo-2
Lo-1
Telo.
Wnts
Wnt2b
Wnt4
Wnt5a
Rspondins
Rspo1
Rspo2
Rspo3
Telo. Lo-1 Lo-2
Wnt Inhibitors
Sfrp1
Frzb
Dkk2
Dkk3
Wif1
Bmp Signaling
Bmp2
Bmp4
Chrd

Figure S3. Three distinct PDGFRA^{+} mesenchymal cell populations (Related to Figure 3)**.**

(A) Distributions of *Pdgfra* and *Cd34* mRNA expression in three PDGFRA^{+} cell types identified by scRNA-seq: telocytes and two PDGFRA^{lo} subpopulations, Lo-1 and Lo-2. Projection of *Foxl1* levels onto the t-SNE map verifies exclusive expression in telocytes. Heat scale is the same for all t-SNE plots in this figure.

(B) Projections on the t-SNE map of all Wnt, Rspo, Wnt inhibitor, and BMP-pathway transcripts detected in ensemble mRNA profiles (Table S1). *Rspo3* is also depicted in a violin plot, as an example, showing comparable expression in Lo-1 and Lo-2 cells, but not in telocytes.

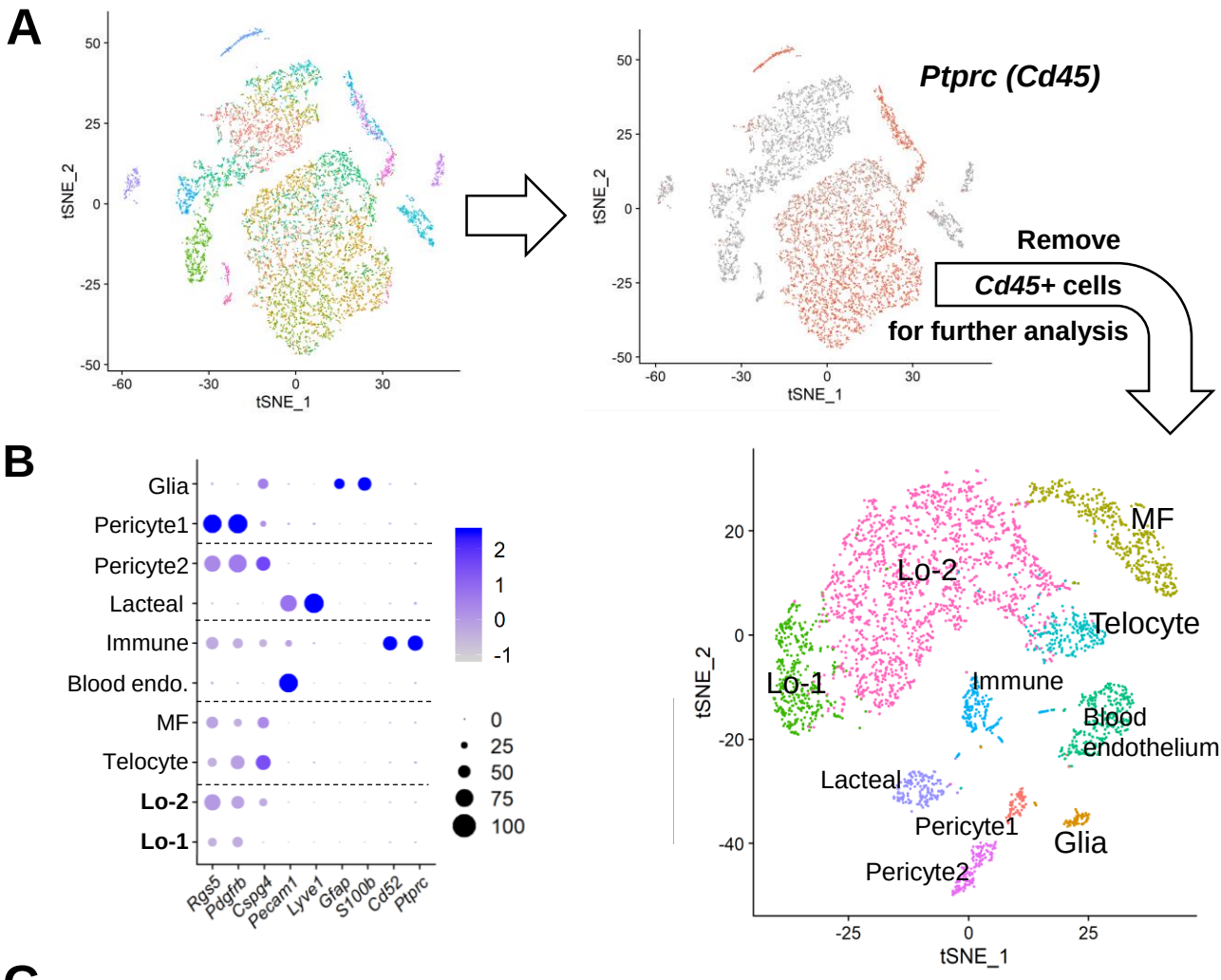

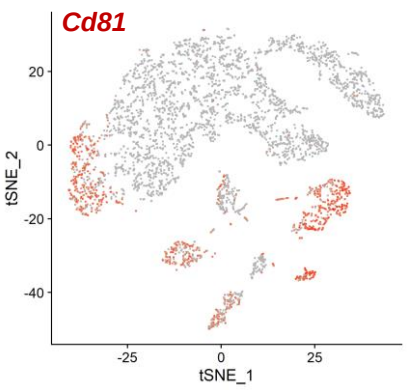

gene	ISC	Paneth	Ent.	Telocytes	PDGFRA^{lo}	EC	LEC
Cd81	582	155	301	5	179	782	860
Cd34	0	0	0	9	536	180	16
Tbp	20	12	24	16	13	13	19

Average RPKM values from bulk RNA-seq (rounded to nearest integer)

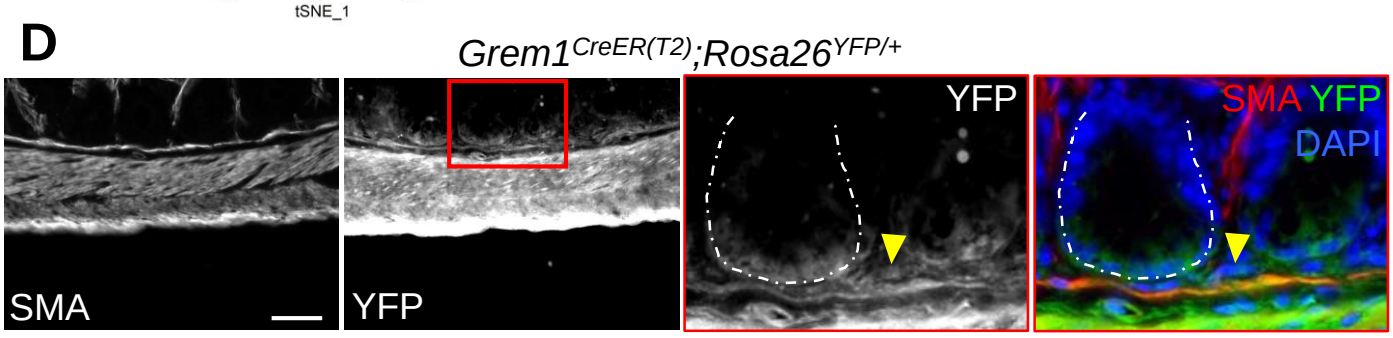

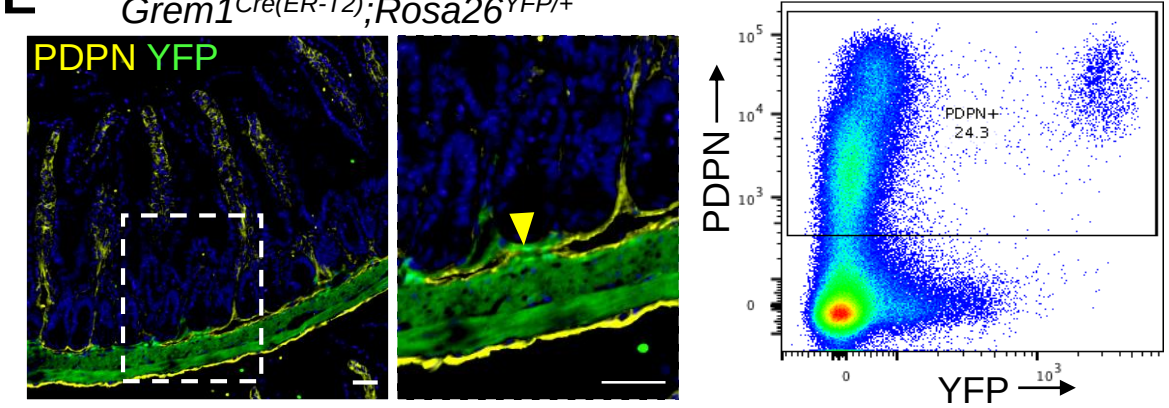

Figure S4. Characterization of small intestinal mesenchyme at single-cell resolution **(**Related to Figures 4 and 6)**.**

(A) t-distributed stochastic network embedding (t-SNE) of scRNA-seq data from 9,353 cells (left) and projection of *Cd45* (*Ptprc*) expression onto the tSNE template. Removal of these *Cd45*$^{+}$ leukocytes, followed by re-clustering of cells, revealed 10 resident stromal cell populations.

(B) Expression domains of known marker genes allow assignment of resident stromal cell types.

(C) Projection of *Cd81* mRNA levels on the t-SNE plot from whole mesenchyme reveals multiple expressing populations, confirming the results from bulk RNA analysis (average reads per kilobase per million sequence tags, RPKM values). *Cd81* robustly distinguishes Lo-1 from Lo-2 cells (Fig. 3), but its role as a selective marker is confined to PDGFRA^{lo} cells.

(D) Grem1$^{CreER(T2)}$ activates expression of Rosa26^{YFP} in sub-cryptal mesenchymal (arrowhead) and external smooth muscle cells. SMA immunostain and YFP fluorescence are shown in the 2 left images. In the 2 right panels, signals within the red box are magnified and merged. Fluorescent signal within crypt epithelium is background. Scale bar, 50 μm.

(E) In addition to the external smooth muscle, *Grem1*$^{CreER(T2)}$*;Rosa26*$^{YFP/+}$ intestines express YFP in sub-cryptal YFP^{+} cells that co-express PDPN (Podoplanin, arrowhead). These cells represent only the sub-cryptal fraction of PDPN^{+} mesenchymal cells; supra-cryptal PDPN^{+} cells (the majority) lack YFP (Grem1) expression. These anatomic findings are mirrored in 2-color flow cytometry with PDPN Ab and YFP.

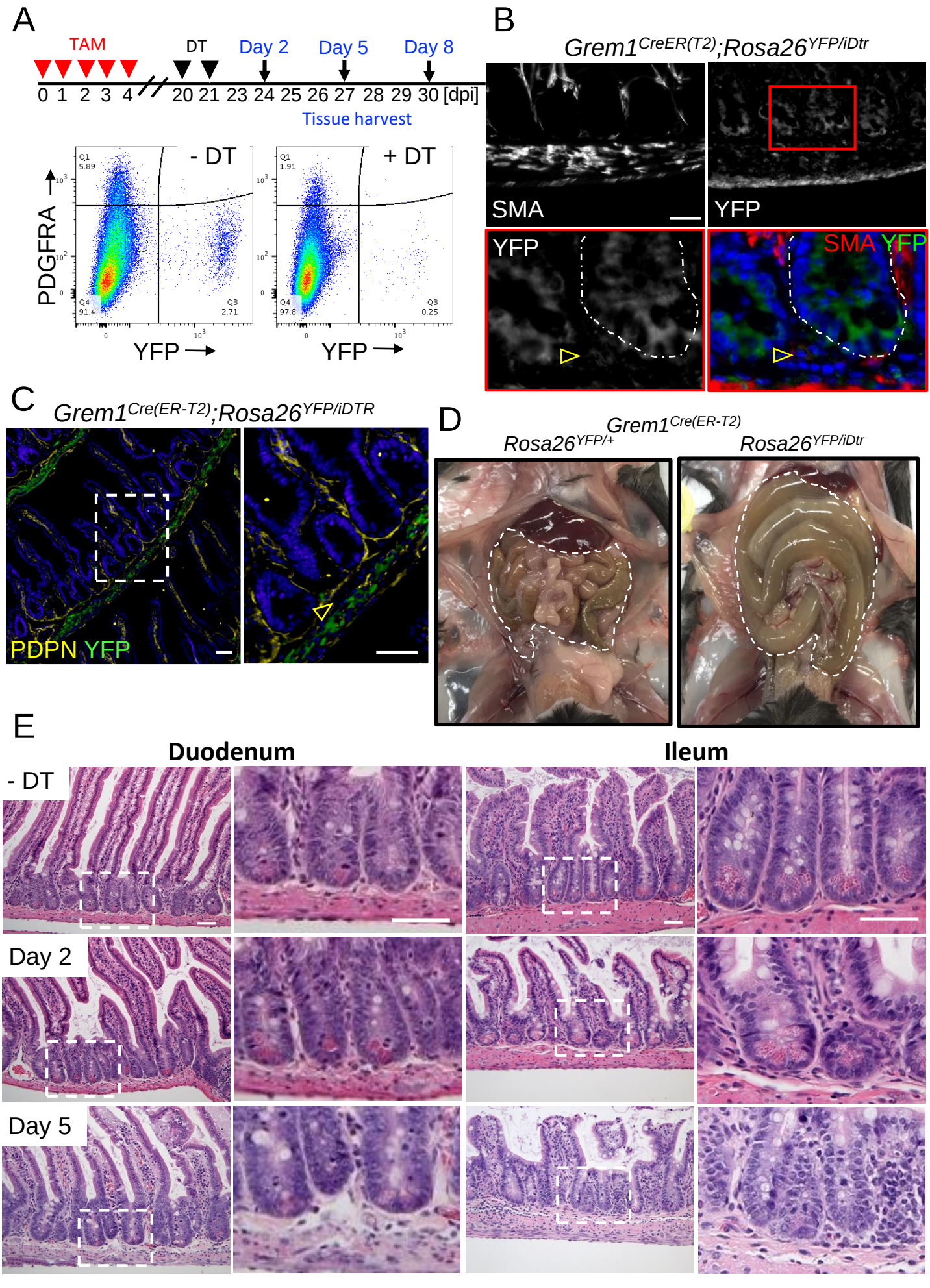
A
TAM
DT
Day 2
Day 5
Day 8
0 1 2 3 4 20 21 23 24 25 26 27 28 29 30 [dpi]
Tissue harvest
- DT
+ DT
PDGFRA
YFP
YFP
B
Grem1CreER(T2);Rosa26YFP/iDtr
SMA
YFP
YFP
SMA YFP
C
Grem1Cre(ER-T2);Rosa26YFP/iDTR
PDPN YFP
D
Grem1Cre(ER-T2)
Rosa26YFP/+
Rosa26YFP/iDtr
E
Duodenum
Ileum
- DT
Day 2
Day 5

Figure S5. Characterization of *Grem1$^{CreER(T2)}$;Rosa26$^{YFP/iDTR}$* mouse intestines after ablation of *Grem1^{+}* cells (Related to Figure 6**).**

(A) Schedule of drug treatments to ablate *Grem1^{+}* cells. Tamoxifen (TAM) was administered on 5 consecutive days to activate CRE recombinase and *Diphtheria* toxin receptor (DTR) expression, followed 15 days later by two consecutive days of DT injection to kill DTR^{+} (*Grem1^{+}*) cells. Intestines were collected 2, 5, and 8 days after the last DT injection. YFP flow cytometry demonstrated efficient ablation of *Grem1^{+}* cells.

(B) Diphtheria toxin (DT)-treated *Grem1$^{CreER(T2)}$;Rosa26$^{YFP/iDtr}$* intestines show loss of external SMA^{+} smooth muscle and of sub-cryptal YFP^{+} cells (empty arrowhead points to site of signals seen in DT-untreated intestines, see Fig. S4D). Crypt epithelial fluorescence is background. Scale bar, 50 μm.

(C) Co-staining of DT-treated *Grem1$^{CreER(T2)}$;Rosa26$^{YFP/iDtr}$* intestines with PDPN Ab confirms loss of sub-cryptal, and preservation of supra-cryptal, PDPN^{+} cells. Empty arrowhead points to site of signals seen in DT-untreated intestines (Fig. S4E). Scale bar, 50 μm.

(D) Intestinal dilation and wall edema in *Grem1$^{YFP/iDtr}$* mice 8 days after treatment with DT. The intestines are outlined.

(E) Hematoxylin and eosin-stained tissue sections from the duodenum and ileum of *Grem1$^{CreER(T2)}$;Rosa2$^{/iDtr}$* mice on different days after injection of DT to ablate *Grem1^{+}* cells. All photomicrographs represent data from 3 or 4 independent experiments and boxed areas in each image are magnified to the right. Note paucity of granular Paneth cells at the crypt base. All scale bars, 50 μm.

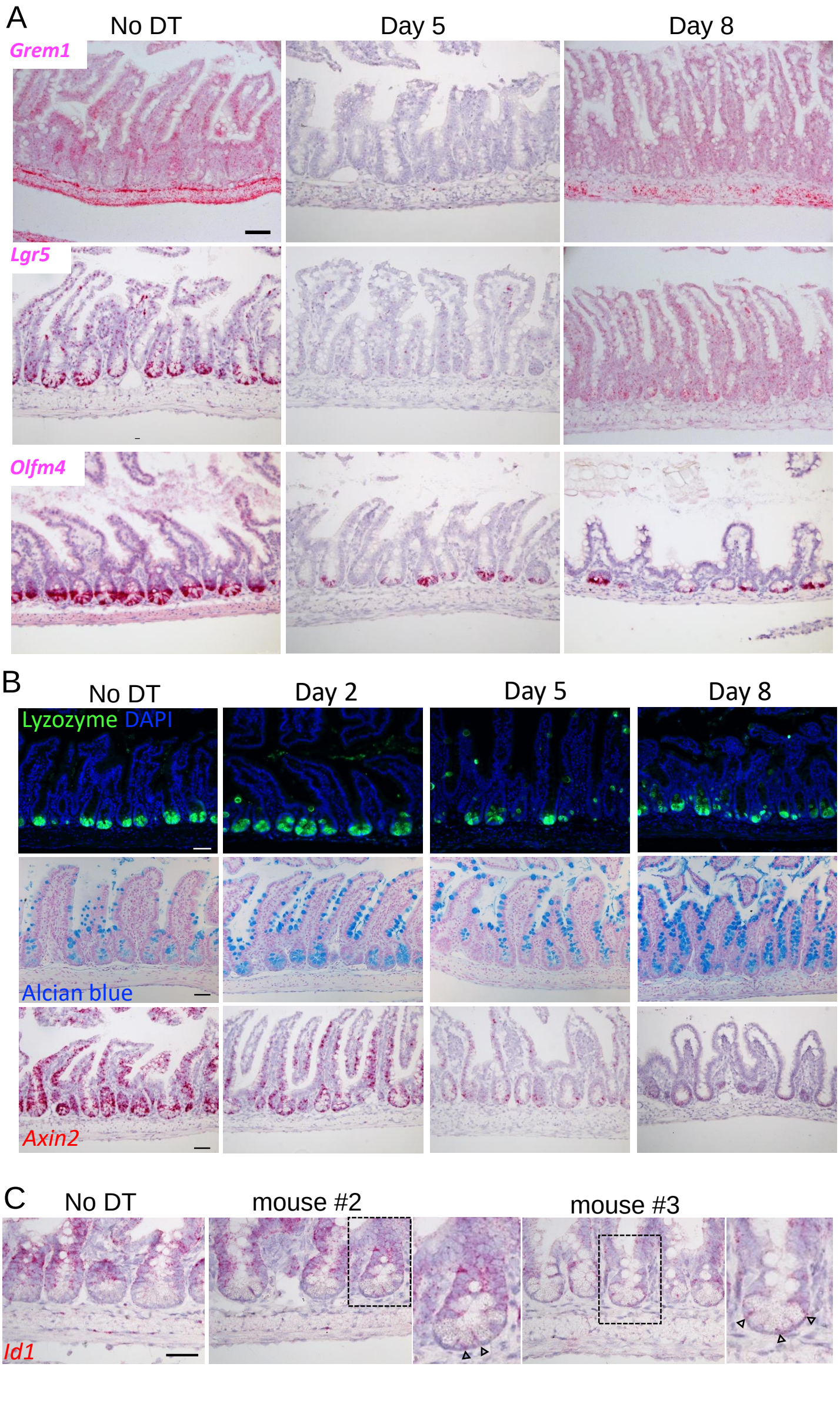
A
No DT
Day 5
Day 8
Grem1
Lgr5
Olfm4
B
No DT
Day 2
Day 5
Day 8
Lyzozyme DAPI
Alcian blue
Axin2
C
No DT
mouse #2
mouse #3
Id1

Figure S6. Loss of Grem1$^+$ cells affects epithelial features (Related to Figure 6**).**

(A) *Grem1* and ISC markers *Lgr5* and *Olfm4*, all detected by RNA in situ hybridization, were absent or markedly reduced throughout the period of observation, here shown at 5 and 8 days after administration of DT.

(B) Paneth cells, detected by LYZ1 immunostaining, were reduced in numbers at the crypt base and occasionally mislocalized in higher crypt tiers. These defects were not observed at 2 days, but apparent 5 and 8 days after administration of DT. Goblet cells, marked by alcian blue stain, were increased in number, especially by 8 days after DT treatment. *Axin2* mRNA (in situ hybridization), present in much of the crypt and some villus cells in untreated ileum, was progressively reduced after ablation of *Grem1*$^+$ cells. All images represent data from 3 or 4 independent experiments.

(C) Additional in situ hybridization images from day 2 after DT treatment show pervasive Id1 expression in crypt base columnar cells in 3 independent animals. Scale bars, 50 μm.

A

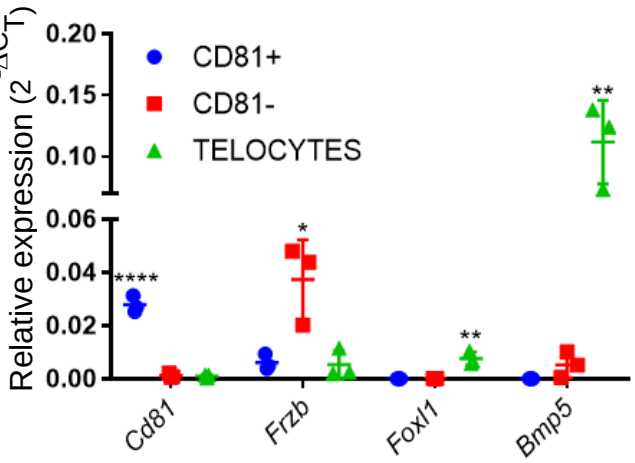

CD81_F	ACACCTTCTACGTGGGCATC
CD81_R	TGCTTCACATCCTTGGCGAT
Frzb1_F	TGCAAATGTAAGCCTGTCAGAGC
Frzb1_R	TCCACAACGGCGGTCACATC
Foxl1_F	TCATCATGGATCGCTTCCCG
Foxl1_R	CCTCTTCCTGCGCCGATAAT
Bmp5_F	TAGATGTGGGCTGGCTTGTC
Bmp5_R	ACCTCGCTTGCCTTGAAGAA

B

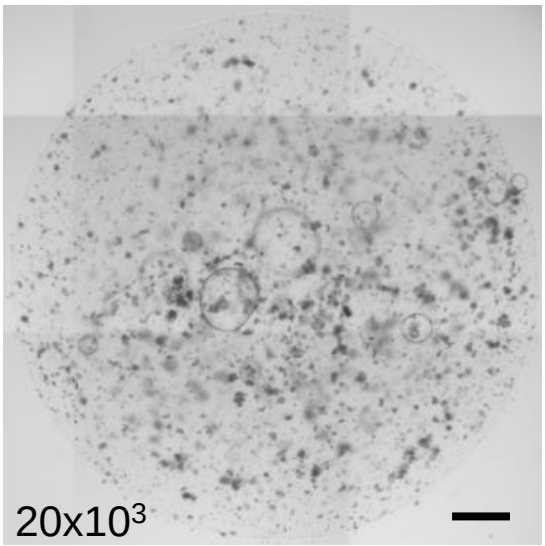

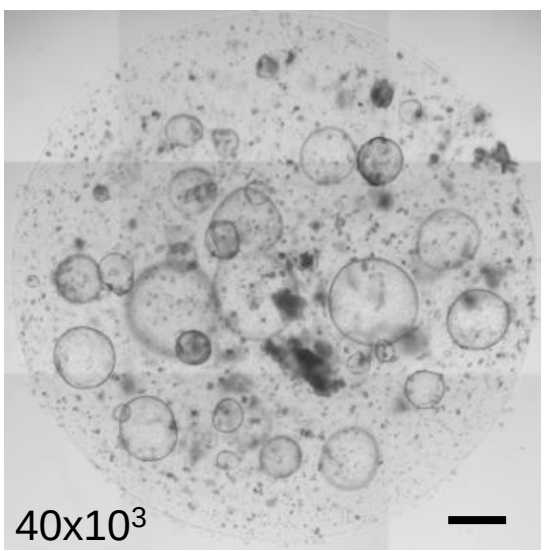

C

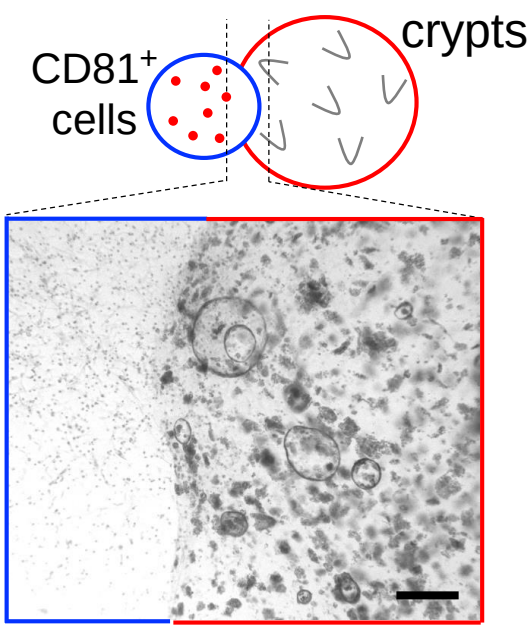

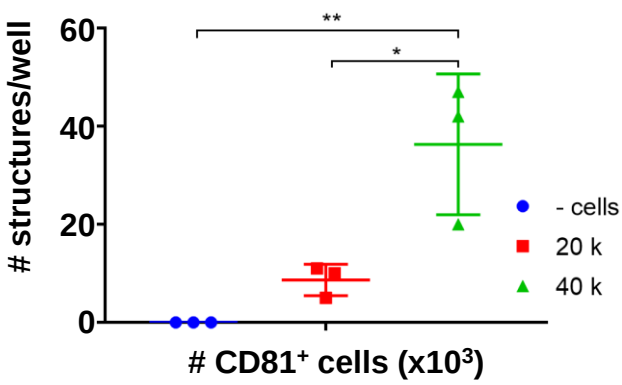

D

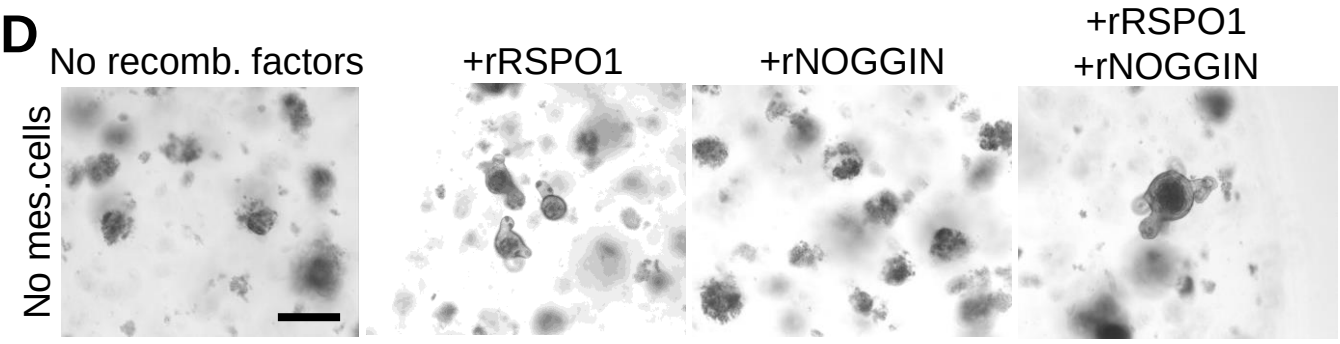

E

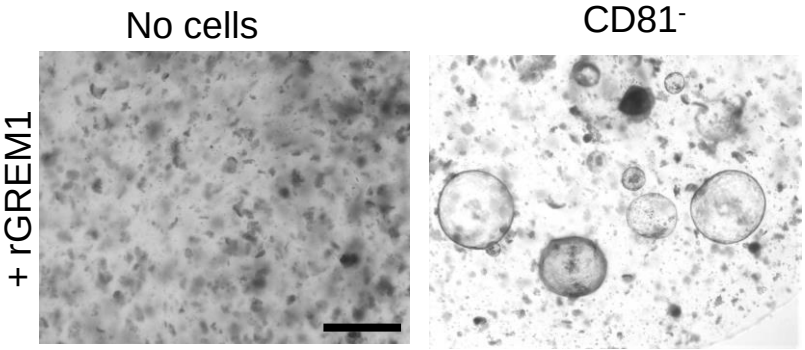

Figure S7. Enteroid growth supported by CD81^{+} PDGFRA^{lo} cells (Related to Figure 7)**.**

(A) qRT-PCR analysis of PDGFRA^{+} cell markers, relative to *Gapdh*, in FACS-purified CD81^{+}PDGFRA^{lo} (Lo-1) and CD81^{-}PDGFRA^{lo} (Lo-2) cells and telocytes cultured for 3 days before crypt co-cultures. Forward (F) and reverse (R) primer sequences are shown below.

(B) Enteric spheroid growth increased with the number of CD81^{+}PDGFRA^{lo} cells in crypt co-cultures in the absence of recombinant growth factors. Scale bar, 1 mm. The graph depicts results from 3 independent experiments. Significance of differences (one-way ANOVA) *p<0.05, **p<0.01.

(C) Culture of CD81^{+}PDGFRA^{lo} cells (Lo-1, left, blue) and isolated crypt epithelium (right, red) in separate, adjoining collagen drops without recombinant factors. Abundant spheroids grew at the interface of the two drops, indicating diffusion of trophic material from the mesenchymal population (N=3). Scale bar, 250 μm.

(D) Without mesenchymal cell support, isolated crypts produced few small organoids in the presence of rRSPO1 alone, none in the presence of rNOGGIN alone, and robust budding organoids when both factors were provided (N=4). Scale bar, 500 μm.

(E) Enteroid formation in crypts co-cultured with Cd81^{-}PDGFRA^{lo} cells and rGREM1 (N=3).